-RESEARCH PAPER-

International Journal of Mining and Geo-Engineering

IJMGE

IJMGE 57-2 (2023) 159-169

DOI: 10.22059/IJMGE.2022.347447.594993

Geochemical prospectivity of Cu-mineralization through concentration-number fractal modeling and prediction-area plot: a case study in East Iran

Ashkan Saydi [a], Maysam Abedi [a], Abbas Bahroudi [a,*], Hossain Ferdowsi [a]

[a] *School of Mining Engineering, Faculty of Engineering, University of Tehran, Tehran, Iran.*

Article History:

Received: 20 August 2022.

Revised: 29 November 2022.

Accepted: 17 December 2022.

ABSTRACT

The Birjand region is a part of the South Khorasan province, situated in the structural-magmatic zone of eastern Iran. As a part of the continental shelf, it forms from subduction during the Cenozoic and subsequent continental collisions. This region is favorable for copper and gold mineralization for various geological reasons. The ultimate goal of this study is to create a Cu geochemical potential map to delimit prone regions for further mining activities. A total of 2468 geochemical samples were gathered to run a 20-element analysis. Taking data preprocessing approaches such as correction of outlier data and data normalization into consideration, a fractal graph through Concentration-Number (C-N) model was produced to isolate different geochemical populations of Cu, Pb, Zn, Ag, Ba, and Ni for Cu targeting. Then, a Prediction-Area (P-A) graph was plotted for each geochemical variable to determine the weight of each evidence map. The results show that Barium map indicates a prediction rate of 72% and specifying 28% of the studied areas as mineralization prone areas. The zinc geochemical map presents an ore prediction rate of 65% and 35% of area as potential zone. In addition, copper with an ore prediction of 56% covered 44% of the Birjand region. Finally, a hybrid evidence map was overlaid. Accordingly, the geochemical potential areas are further located towards the south and south-east of Birjand, which are closely related. Moreover, there are highly favorable areas in the middle part. It is noteworthy that the copper potential map has higher efficiency over each individual geochemical evidence, with an ore prediction rate of 75% and occupying 25% of the area as favorable zones.

Keywords: *Concentration-Number fractal (C-N), Prediction-Area fractal (P-A), MPM, Cu, Birjand.*

1. Introduction

Porphyry deposits have been generally known since the 1920s as low-grade, high-tonnage deposits, and none of the porphyry copper deposits were mined until 1905. The formation of these deposits is directly related to hydrothermal systems connected to intrusive masses. Therefore, their deposit model is in the form of veins as well as diffusion, and in the current situation, even low grades, such as 0.2-0.5% are considered economical. One of their characteristics is the construction of sulfide-silicate zones, as presented by Lowell and Gilbert (1970) [1]. Around many porphyry copper deposits, traces of gold, silver, lead, zinc, and manganese are likely to be present, and gold and even extracted molybdenum are commonly considered as by-products. The rocks found in the mineralization areas of porphyry copper are from granodiorite, tetalite, and quaterzmonzonite to diorite. The related alterations from inside to outside respectively include: potassic, phyllite, clay, and propylitic.

Although there are not many studies to find porphyry deposits in the studied area, considering the geological structures of the Birjand region, and this region is located almost on the porphyry mineralization belt of Iran, which starts from the north-west and continues to the south-east, the possibility of occurrence of porphyry deposits in this area is very high.

Separating geochemical anomalies from the background is a helpful method for geochemical exploration. Anomalous thresholds, the most beneficial criterion for cross-checking information with numerical data from different sources, are commonly used in geochemical studies [2-4]. Predictive model of mineral capacity using the Geographic Information System (GIS) is a valid and accepted tool for drawing the goals of mineral exploration that are reproducible. Abnormal geochemical areas can be defined by more than a particular threshold value. Different statistical methods are used to determine the values of anomaly threshold based on a specific assumption on statistical distribution of geochemical variables. Separation of geochemical provinces concerning the purpose of the mineral deposit, has attracted the attention of scientists [5-7]. Recognizing and separating the anomalous areas from the background is an integral part of geochemical exploration research [8-9].

Different versions of fractal/multi-fractal modelling, developed by Mandelbrot (1983) [11], have been proposed to analyze geochemical data. Numerous studies have been done on the use of these versions: number-size (N-S) by Mandelbrot (1983) [11], concentration-area (C-A) by Cheng et al. (1994) [12] and Farhadi et al. (2022) [13], distance-concentration (C-D) by Li et al. (2003) [10], spectrum-area (S-A) by Koohzadi et al. (2021) [14] and Pourgholam et al. (2022) [15], concentration-number (C-N) by Shahbazi et al. (2021) [16] and Torshizian et al. (2021) [17], concentration-distance to fault structures (C-DF) by Nabilou et al. (2021) [18], concentration-volume (C-V) by Mahdizadeh et al. (2022) [19] and Afzal et al. (2011) [20,21]. One of the

* Corresponding author. *E-mail address:* bahroudi@ut.ac.ir (A. Bahroudi).

main features of fractal models compared to common statistical methods is considering the spatial variations of informational samples [12; 22-24], which reflects the geological, geochemical, and mineralogical sequences of a region [9-10]. Based on fractal analysis [25-26], geochemical indicators can be deduced to prepare the mineral potential map (MPM). In MPM, the location of known deposits can be used to evaluate the performance of predictive models. This is achieved by covering mineral deposit sites on an exploratory classified model [27-29].

MPM is a multi-criterion decision-making (MCDM) function that aims to map and prioritize suitable areas to identify undiscovered mineral reserves of the desired type [27]. Bonham-Carter et al. (1989) [30] used the weight of spatial index classes divided by their respective area covered (area occupied by each class of proven values) to estimate the probability of discovering mineral deposits in several classes, primarily by fractal analysis. Yousefi and Carranza (2015, 2016) [28,31] developed the Prediction-Area Chart (P-A), which the percentage of known deposits predicted by the predictive layers (predictive rate) and the desired areas of the respective predictive classes help to determine the comparative importance of different predictive models. By plotting the P-A diagram, both the deposit rate and the desired region for the exploration targets' mineralization, help to evaluate the predictive models [28; 32-37]. Therefore, if two different predictive models plot exploratory targets with different desired regions but the same prediction value, the model's performance with smaller target areas is higher than the model with larger target areas [37]. Kreuzer et al. (2020) [38] applied MPM to exploration targets and suggested some solutions for future fundamental practical issues which limit the effectiveness of MPM. Some of these issues are the failure of importing data uniformly and objectively representing the search space of interest, as well as difficulty in mapping critical targeting-relevant geoscientific elements in the available or obtainable datasets. Yousefi et al. (2021) [39] tried to enhance mineral exploration targeting using GIS and they do it by (1) reviewing the fundamental aspects of MPM, (2) identifying significant deficiencies of MPM, and (3) discussing possible solutions to alleviate or eliminate these deficiencies.

Geochemical evidence maps should be generated using logistic functions before drawing P-A diagrams and fractal curves [28]. The values of spatial evidence in each map are changed using a logistic function, because it can correctly convert absolute values to the range [0,1] [40]. Therefore, using a logistic function prevents the disadvantage of data-driven approaches to MPM in terms of exploratory trends and random error in mapping areas generally depicted around known mineral events [28].

The primary purpose of this study is to identify geochemical anomalies in the Mokhtaran, Basiran, Deh-Salam, and Kardegan areas under a single map using samples of stream sediments. Through multivariate analysis of geochemical clustering data and principal component analysis (PCA), after pre-processing all input elements, several indicators are prepared to be displayed at intervals indicating the usefulness of Cu potential mapping. Simultaneous consideration of the C-N fractal curve and the P-A diagram provides information about the data-driven weight of each indicator map concerning Cu events. Finally, a multi-layer index overlay map is created to guide the Cu event further.

2. Geology of the study area

Agha-Nabati (2005) prepared the structural zoning map of Iran (Figure 1) [41], in which the study area is specified. The map of the study area (Figure 2) includes four maps: Basiran (the right one in the middle third), Kardegan (the left one in the middle third), Mokhtaran (in the upper third), and Deh-Salam (in the lower third) that each of these maps was prepared in a 1: 100000 scale by the Geological Survey of Iran. In terms of the geological and tectonic characteristics of the Mokhtaran region, situated in the southern part of Birjand city and located in South Khorasan province, this region has good potential for the occurrence of porphyry copper and epithermal gold ores. Most of the locations that have been identified or exploited in this area as metal deposits have been studied by field surveys. Due to the high altitude of these areas and their inaccessibility, further work is still needed. Therefore, using methods, such as remote sensing alongside surveys, significant progress can be made in identifying undiscovered reserves. The presence of young intrusive masses in the region, such as Microgranodiorite, as well as the presence of Paleogene volcanic as hosts, are essential indicators of epithermal gold and porphyry copper mineralization in the region. Significant alterations that represent porphyry copper and epithermal gold mineralization include, propylitic (calcite, epidote, and chlorite minerals), argillic, sericitization, and iron oxides (goethite, hematite, and lepidocrocite).

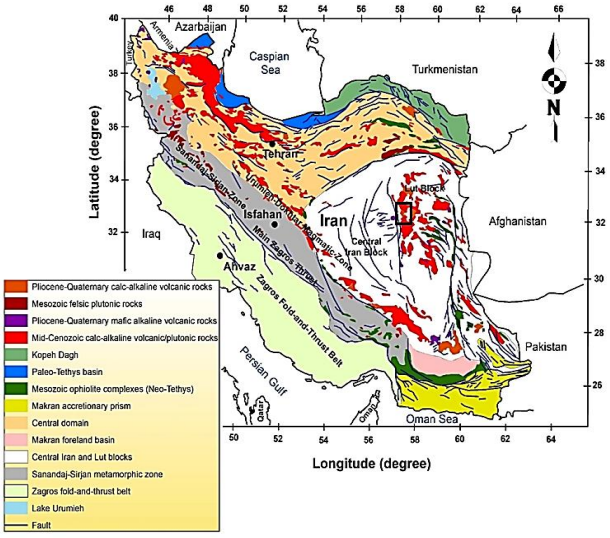

Figure 1. Structural geological map of Iran on which the location of the study area is specified (reproduced from Richards et al. (2006) [57]).

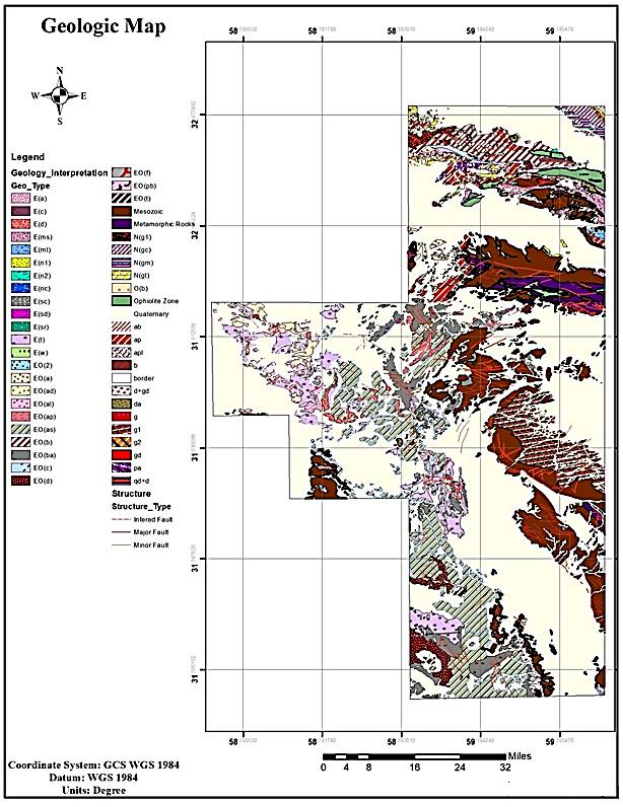

Figure 2: Geological map of the study area in 1:100,000 scale consists of the areas of Basiran (middle third-right), Deh-Salam (lower third), Kardegan (middle third-left) and Mokhtaran (upper third).

In the Basiran region, due to its unique geological conditions and many magmatic activities in different geological eras, different types of mineralization, such as epithermal, porphyry, and veins can be found. For instance, the Qale-Zari copper-gold mine can be mentioned. The eastern and central parts of this region are mostly covered by Mesozoic and Tertiary volcanic sediments and volcanic rocks. The rock units of the Basiran region can be divided into five groups: sedimentary rocks, deep and semi-deep igneous rocks, lavas, pyroclastic rocks, and skarns [42]. The oldest stratigraphic unit in the study area is Jurassic shale and sandstone. The Paleocene base conglomerates are brown and massive, and thick cream-colored limestones containing Paleocene microfossils are metamorphosed on lava and sandstone lavas and pyroclastic rocks belonging to the Eocene [42] which are cut by the semi-deep and deep range stones. In some parts of this area, Neogene conglomerates up to a thickness of about 50 m are located on Eocene lavas and tuffs. Massifs, such as granodiorite, granite, and diorite are exposed in different parts of this region, attributed to the Mesozoic and Tertiary geological periods.

Most of the Deh-Salam region is covered by volcanic rocks from the third era with a significant andesitic-dacite composition, which is a reason for the various parts to be covered by sand and volcanic rocks with a dark appearance. The rocks of this region can be divided into internal and external forms. The inner rocks include granophyre, quartzsienite, and syenite, which have undergone potassium, silicic and sercitic alterations, and green diorite is seen at the heights of the region. The external rocks in this area include basaltic andesite with grayish-green color and dacite with a cream to pink color; all the outer rocks of the area have been affected by argillic, propylitic, and siliceous alterations.

In the Kardegan region, intense and continuous volcanic activity in the Middle Jurassic can be named the most important geological activity, along with landslide faults and gentle folds. From the old layers of this area, shale, sandstone, and Lower Jurassic to Upper Cretaceous limestones can be found, which have been severely wrinkled in some areas. Some of the rocks in the Kardegan area have transformed into slate and schist. The Intrusive and exclusive igneous rocks of this region include from Eocene to Oligocene. As one of the igneous units, dark basaltic lavas are the most widespread in the region. Among the igneous rocks can be pointed the units with almost acidic rocks, such as dacite and rhyolite with a porphyry texture, and basalt to acidic tuffs, all three of these are part of the extrusive igneous rocks. The only intrusive igneous units are diorite and granodiorite rocks, which are covered by Quaternary alluvium, and only small protrusions of them can be seen in the region.

In the Birjand region, a significant volume of magmatism activities in the form of volcanic events and the placement of intrusive masses has been done due to subduction. Most of the magmatism in eastern Iran consists of Eocene-Oligocene volcanic rocks exposed in the form of lava and igneous rocks. In this area, there are intrusive masses of granodiorite, quartz diorite, and diorite with Eocene age, as reported in the Urmia Dokhtar belt. In addition to these intrusive bunches, volcanic rocks of basalt type, ranging from “andesitic basalt to andesite”, and their associated pyroclastic have been reported. There are some igneous rocks in the form of stocks within volcanic units in the region. These stocks do not have significant outcrop metamorphism. These stocks can also be seen as outcrops with high morphology and rocks. Pyroclastic and volcanic deposits are commonly seen on and around stocks. Geochemical and petrological evidence suggests that these igneous massifs formed in a subduction zone. There is evidence of magmatic mixing between the submerged lithosphere and crustal rocks. In general, the intrusive masses are petrologically classified in the calc-alkaline to shoshonitic series, and they characterize the continental arc environment with an enriched mantle origin along with the effect of subduction-zone fluids.

As a result of magmatic activity and subsequent events, various minerals, such as copper, molybdenum, gold, and silver have been formed. Some of these minerals are in the form of veins, massive sulfides, and skarn deposits, while others have been reported as porphyries. In the study area, some lead, zinc and manganese occurrences have been identified. However, the copper index has not been found, while there are 12 active mines in this section, but some of these mines do not have copper mineralization. Therefore, after the introduction of the mines, the mines with copper mineralization are investigated according to the produced/generated data. There are active mines in the Mokhtaran region that have copper mineralization as well as other minerals. The Khonik mine is a low sulfide epithermal mine whose mineralization is gold, silver, copper, and boron, located in the geological unit of volcanic and agglomerated sections of the Eocene period.

The Copper-Gold mine of Chah-Zaghoo is a porphyry-skarn type, with granite as its host rock. In the Kardegan area, there is a well-known porphyry copper deposit called Chah-Shalghami, which is located in the andesite basalt and gray to black basalts. The Qale-Zari mine, situated in andesitic lavas, semi-deep equations, and tuff, is an (IOCG) mine whose main ores are Copper and Gold.

Table 1 shows the geological descriptions of the abovementioned area shown in Figure 2.

3. Research method

In this study, after utilizing conventional statistical methods, such as drawing histogram and box plot distribution functions, factor analysis as an important multivariate statistical method was applied. Factor analysis which is a powerful multivariate statistical approach has been implemented on the data. By reducing the dimensions of variables (elements), the main factor affecting on mineralization was obtained. After that a concentration-number fractal filter was implemented on the data to better and clearly separate anomalies from the background.

Finally, data-driven weight assignment to each indicator map was determined through P-A plots, which amplifies final index overlay map for introducing favorable zones of Cu occurrences.

3.1. Geochemical data analysis

Table 2 contains statistical properties, such as the number of samples in the region for each of the studied elements, their maximum and minimum values, and the mean and standard deviation of those elements, including copper, lead, zinc, silver, barium, and nickel. The histograms of geochemical concentration distribution are shown in the left column of Figure 3, and their box diagrams are shown in the right column, which plan to eliminate outlier data for a better geochemical potential map. Moreover, by simultaneously examining the histogram of geochemical concentration distribution and box diagrams, general geochemical information about the distribution of the data in terms of concentration is obtained.

In this area, there are 2468 geochemical data that were analyzed for the gold element by Fire Assay Analysis, and the analysis of the rest of the elements was done by the ICP-OES method. In each of the four areas, the data were collected by different data collector groups, and according to the locations of all the data, they are consistent with waterways so it can be said that the samples were collected by the stream sediments method. Except for the Deh-Salam region, where the accuracy of data collection is 0.001 ppm, in other areas, were collected with an accuracy of 1 ppm.

Multivariate statistical methods are widely used in studying geochemical models. These methods are capable of classification and ranking of geochemical anomalies [43]. For example, we can check the correlation coefficient between the elements, which can determine the relationship between the elements and the main variables related to the mineralization area. The correlation between the elements can also be investigated using the clustering method [44-45], which shows sthe correlation between 17 geochemical variables in this study in the dendrogram of Figure 4. In the next section, the relationship between the copper element and 17 other chemical variables is determined using the Pearson method, which can be seen in Table 3. In the dendrogram plot, the most significant correlation of the copper is with strontium and lead, barium, zinc, and silver in the next stage. In contrast, by the values obtained from the Pearson correlation coefficient, it has the highest

correlation with silver (0.751), and then with lead (0.717) and in the next stage it shows a high correlation with tin, nickel, cobalt, zinc, chromium, barium and antimony elements.

Table 1. Geological structures in the area.

Structure Description	Structure Abbreviation
Andesitic lavas	E_a
Conglomerate	E_c
Dacitic lavas	E_d
Sandstone and Marl	E_{ms}
Sandstone and Marly green tuff	E_{mt}
Primary monolithic limestone	E_{n1}
Secondary monolithic limestone	E_{n2}
Nomolytic conglomerate	E_{nc}
Sandstone and Conglomerate	E_{sc}
Sandy limestone and Sandstone	E_{sd}
Red sandstone	E_{sr}
Conglomerate, Sandstone and Marly red tuff	E_t
Flow tuff	E_w
Andesite	EO_a
Andesite, Dacite and Altered tuff	EO_{ad}
Altered acidic volcanic rocks	EO_{al}
Andesite Porphyry	EO_{ap}
Andesitic lavas, equivalent to semi-deep and tuff	EO_{as}
Volcanic breccia and agglomerate	EO_b
Basalt andesite and Basalt in dark gray to black	EO_{ba}
Conglomerate	EO_c
Dacite	EO_d
Pyroclastic rocks (Volcanic tuff and breccia)	EO_{pb}
Tuff and red Marl	EO_t
Mesozoic rocks	Mesozoic Rocks
Metamorphic rocks	Metamorphic Rocks
Freshwater limestone	Ng_l
Conglomerate	Ng_c
Marly Gypsum	Ng_m
Marly Tuff	Ng_t
Ophiolite Zone	Ophiolite Zone
Quaternary rocks	Quaternary Rocks
Hornblende Andesitic	ab
Pyroxene andesitic	ap
Aplitic microgranite	apl
Basalt	b
Granite + Granodiorite and Monzonite	$d + gd$
Dacite and Microdiorite with Andesite	da
Granite	g
Granite	g_1
Granite (Eocene and Oligocene)	g_2
Microgranodiorite	gd
Andesite Porphyry	pa
Quartz monzonite, Quartz diorite and Oligocene Diorite	$qd + d$

Table 2. Statistical characteristics of the most important elements (ppm) of paragenesis related to copper mineralization.

	Number	Min.	Max.	Mean	Standard Deviation
Cu	2468	9.400	760,000	32.6500	623.809
Pb	2468	4,000	220,000	919.620	10.0715
Zn	2430	20,000	117,000	69.9400	618.792
Ag	1681	0.000	4,000	0.3543	9.4610
Ba	1966	141,000	1011,000	343.8357	969.810
Ni	2468	4,000	550,000	61.8708	41.6324

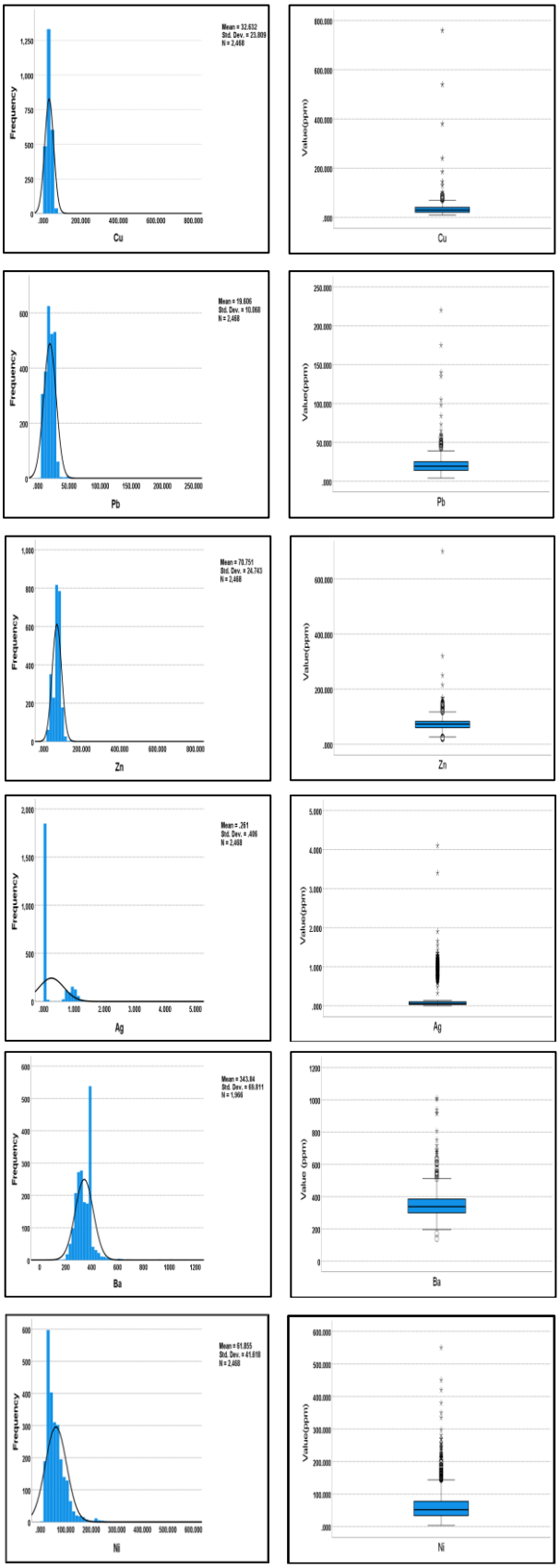

Figure 3. Statistical graphs consisting of geochemical concentration distribution histogram (left column) and box diagram (right column) for copper (row 1), lead (row 2), zinc (row 3), silver (row 4), barium (row 5) and nickel (row 6), respectively.

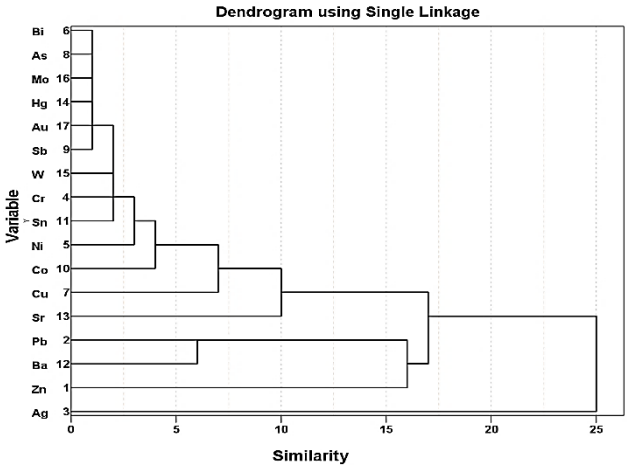

Figure 4. Dendrogram analysis of element concentrations in the study area.

Factor analysis or "principal component analysis (PCA)" is a dimension reduction tool in statistical analysis [46-48], which has attracted the attention of researchers to find the main factors showing the most variability among several geochemical variables. Multivariate statistical analysis, especially factor analysis, is a suitable technique for understanding behavioral characteristics and reducing the number of geochemical variables. Factor analysis has been broadly used to interpret geochemical data obtained from stream sediments [10; 49-51]. The ultimate goal of factor analysis is to explain the types of multivariate data by as many factors as possible and to identify the hidden multivariate data structure. Factor analysis is suitable for interpreting the inherent variability in a geochemical data set with a large number of input elements being analyzed. As a result, factor analysis is often a powerful tool for analyzing exploratory data [10].

To reduce the number of variables, factor analysis has been performed on the geochemical data of the stream sediments, where Table 4 lists six elements and three main components/factors. The elements selected for executing the PCA are based on the previous two methods, as well as considering paragenesis associated with copper in most deposits. The main variables for each factor are determined based on the values obtained in each component, which in the first factor are: copper, lead, and silver, in the second factor are barium and nickel, and in the third factor is the element zinc. As can be seen in the results of the PCA in Table 4, the main factor C1 represents the most variability of elements, such as copper, lead, and silver, that are geochemically correlated to each other and depict mineralization in the area.

3.2. Concentration - Number fractal analysis

Geochemical data often shows self-similarity and self-affinity, thus can be analyzed by the theory of non-Euclidean fractal geometry. As a result, the anomalous areas are distinguished from the background based on the fractal dimensions. Fractal methods can show the relationship between geological, geochemical, and mineralogical information [3; 6; 25; 52]. Among several versions of fractal methods, the concentration-number (C-N) model can be used to explain how the geochemical population is distributed without pre-analyzing the data [53,54]. This model shows a spatial relationship between the input property and the sample values. The following equation can define the C-N model:

$$N(>\rho) = F\rho^{-D} \quad (1)$$

where ρ is the concentration of the element and $N(>\rho)$ is the total number of samples with a concentration equal to or greater than ρ, F is also a constant, and D is the standard power for the fractal dimensions of the concentration distribution. In addition, an $N(>\rho)$ versus ρ curve in a log diagram represents linear segments with different $-D$ slopes, corresponding to different concentration ranges [52-56].

Table 3. Pearson correlation of coefficient of the most important elements.

Zn	**1.000**																
Pb	**0.610**	**1.000**															
Ag	**0.630**	**0.867**	**1.000**														
Cr	**0.351**	**0.483**	**0.576**	**1.000**													
Ni	**0.413**	**0.615**	**0.649**	**0.639**	**1.000**												
Bi	**0.415**	**0.351**	**0.376**	**0.500**	**0.227**	**1.000**											
Cu	**0.392**	**0.717**	**0.751**	**0.401**	**0.627**	**0.054**	**1.000**										
As	**0.333**	**0.449**	**0.454**	**0.625**	**0.268**	**0.582**	**0.122**	**1.000**									
Sb	**0.463**	**0.604**	**0.661**	**0.655**	**0.359**	**0.504**	**0.420**	**0.694**	**1.000**								
Co	**0.637**	**0.694**	**0.766**	**0.542**	**0.745**	**0.384**	**0.612**	**0.323**	**0.503**	**1.000**							
Sn	**0.573**	**0.802**	**0.902**	**0.634**	**0.682**	**0.417**	**0.683**	**0.507**	**0.615**	**0.776**	**1.000**						
Ba	**0.429**	**0.676**	**0.741**	**0.476**	**0.297**	**0.489**	**0.509**	**0.507**	**0.666**	**0.509**	**0.657**	**1.000**					
Sr	**0.452**	**0.165**	**0.165**	**0.317**	**0.085**	**0.584**	**-0.102**	**0.399**	**0.342**	**0.272**	**0.118**	**0.427**	**1.000**				
Hg	**0.236**	**-0.352**	**-0.405**	**-0.334**	**-0.274**	**0.032**	**-0.320**	**-0.174**	**-0.223**	**-0.076**	**-0.434**	**-0.299**	**0.381**	**1.000**			
W	**0.230**	**0.295**	**0.219**	**0.058**	**-0.028**	**0.052**	**0.175**	**0.160**	**0.207**	**0.071**	**0.286**	**0.211**	**-0.274**	**-0.018**	**1.000**		
Mo	**0.309**	**0.626**	**0.648**	**0.233**	**0.392**	**-0.029**	**0.530**	**0.087**	**0.249**	**0.436**	**0.689**	**0.263**	**-0.504**	**-0.260**	**0.209**	**1.000**	
Au	**0.087**	**-0.096**	**-0.152**	**-0.076**	**-0.050**	**0.060**	**-0.068**	**0.051**	**0.001**	**-0.093**	**-0.235**	**-0.073**	**0.299**	**0.186**	**-0.060**	**-0.171**	**1.000**
	Zn	Pb	Ag	Cr	Ni	Bi	Cu	As	Sb	Co	Sn	Ba	Sr	Hg	W	Mo	Au

Based on the C-N logarithmic diagram, the seven geochemical classes for Copper (Cu) are shown in Figure 5a. It can be said that the anomalous region has a threshold of 0.79, which includes grades above 189.6 ppm, and is *colored in* purple and navy-blue, as shown in Figure 5c.

Based on the results in Figure 6a, seven different geochemical classes can be observed for the Lead variable (Pb), which has a threshold of 0.77 for the anomalous region and considering the last two parts colored in purple and navy-blue. In Figure 6c these abnormal areas in the study area contain grades above 69.3ppm.

As can be seen from the logarithmic diagram of C-N for the variable Zinc (Zn) and according to Figure 7a, there are five geochemical classes. Considering the last population as anomalous values, it shows a threshold of 0.84, displayed in red and contains values above 126 ppm, as shown in Figure 7c.

Table 4. Principal component analysis of the most important elements and display of components.

	C1	C2	C3
Cu	**0.870**	0.024	-0.119
Pb	**0.859**	0.123	0.173
Ag	**0.857**	-0.185	-0.172
Ba	0.440	**-0.749**	0.065
Ni	0.307	**0.648**	-0.586
Zn	0.330	0.492	**0.768**

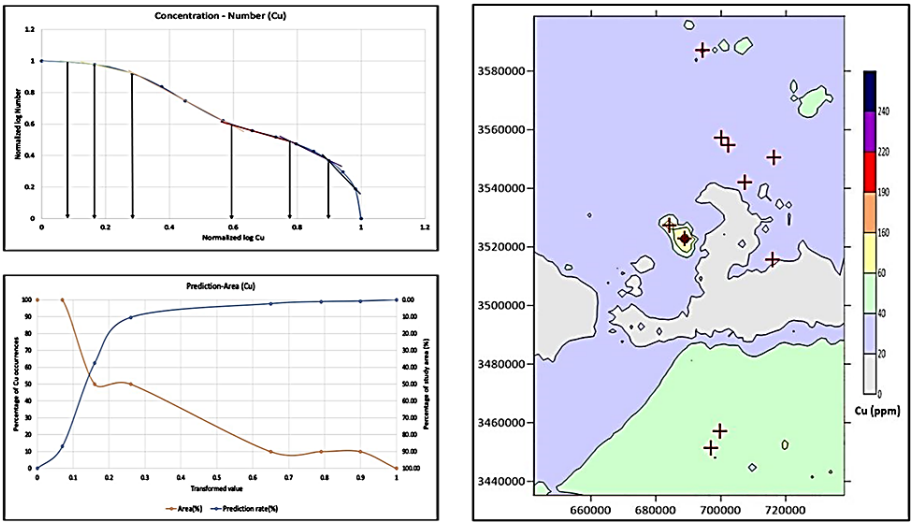

Figure5. Copper geochemical distribution map, (a) full logarithmic graph of Concentration-Number fractal, (b) Prediction-Area diagram, and (c) fractal-based classification map. The extraction weight is equal to 0.24116.

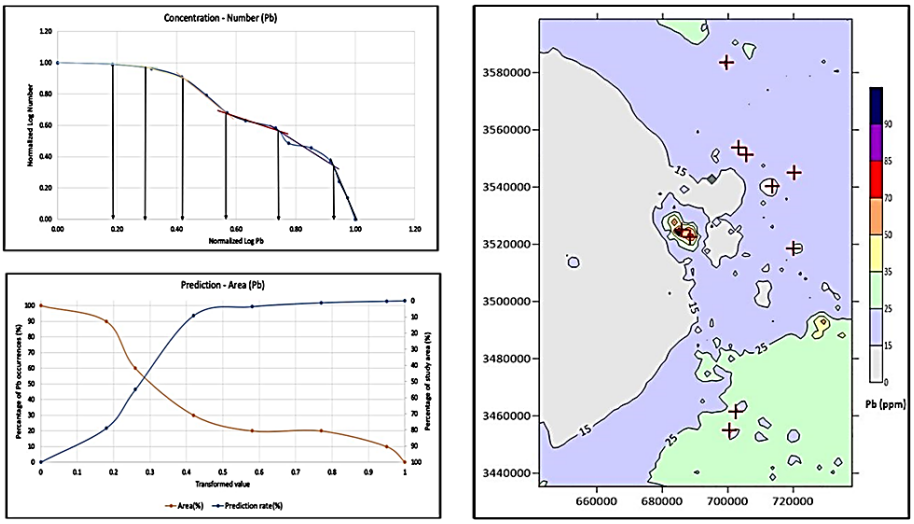

Figure 6. Lead geochemical distribution map, (a) full logarithmic graph of Concentration-Number fractal, (b) Prediction-Area diagram, and (c) fractal-based classification map. The extraction weight is equal to 0.20067.

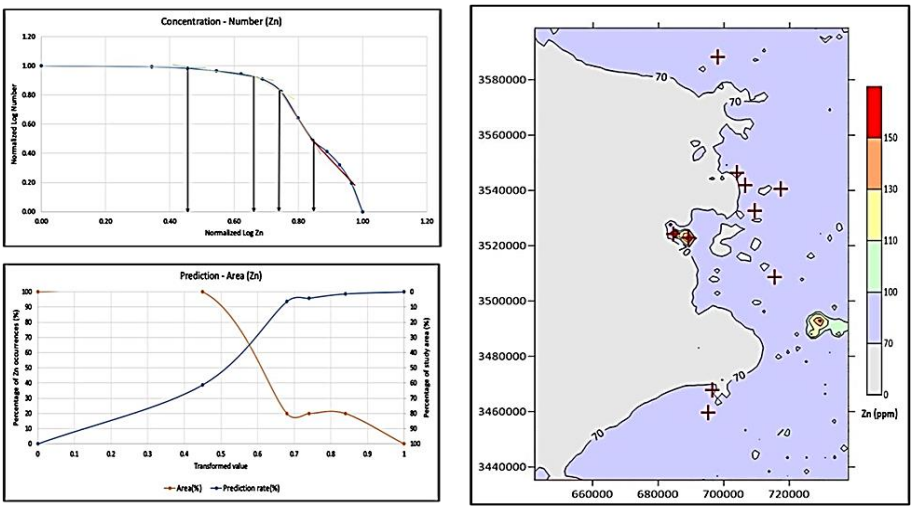

Figure 7. Zinc geochemical distribution map, (a) full logarithmic graph of Concentration-Number fractal, (b) Prediction-Area diagram, and (c) fractal-based classification map. The extraction weight is equal to 0.61904.

For the variable Silver (Ag) in the logarithmic diagram of C-N, six geochemical classes are considered according to the specified trend and their distance. It is observed that the sixth class is the abnormal one, demonstrates the threshold value of 0.92 (Figure. 8a) depicted in red colour (Figure 8-c) that represent grades higher than 1.196 ppm.

Six geochemical classes for the variable Barium (Ba) are shown in the C-N logarithmic diagram in Figure 9a, and according to the studies on the trend and distance between classes from each other, the last two classes are considered abnormal, which show a value of 0.82 on the graph. Note that in Figure 9c on the map drawn in red and purple, it is shown the grades above 459.2 ppm.

Six geochemical classes are considered for the Nickel (Ni) variable in the C-N logarithmic diagram. By viewing the population trends and the difference between them in Figure 10a, only the last class is regarded as an abnormal class and has a value of 0.95. This is also shown in Figure. 10c as a C-N logarithmic diagram in purple, and applies to grades more significant than 228 ppm.

Figure 11 shows the classification map of all elements in two classes. The first class is related to the background values, and the second class is connected to the least anomalous value in the region. These maps are used to determine the location of mines and mineral indices in the study area. In this study, using the two-class maps the accuracy of the full logarithmic fractal diagram of grade-number and the prediction-area diagram for each element was checked.

3.3. Prediction-Area plot

The intersection point value can be used as a threshold in the P-A diagram of the control layers to create a binary evidence map for use in Boolean MPM logic [26]. Most mineral reserves are related to the intersection area up to the maximum values [24]. In MPM, the weights assigned to spatial evidence should reflect the actual spatial relationships between the spatial evidence and the intended mineral reserves. Therefore, known Cu locations can help the reliability of the weights assigned to the spatial evidence, indicating their spatial relationship to mineralization in the Birjand region. There are two curves in a P-A map of an evidence map: the known mineral event

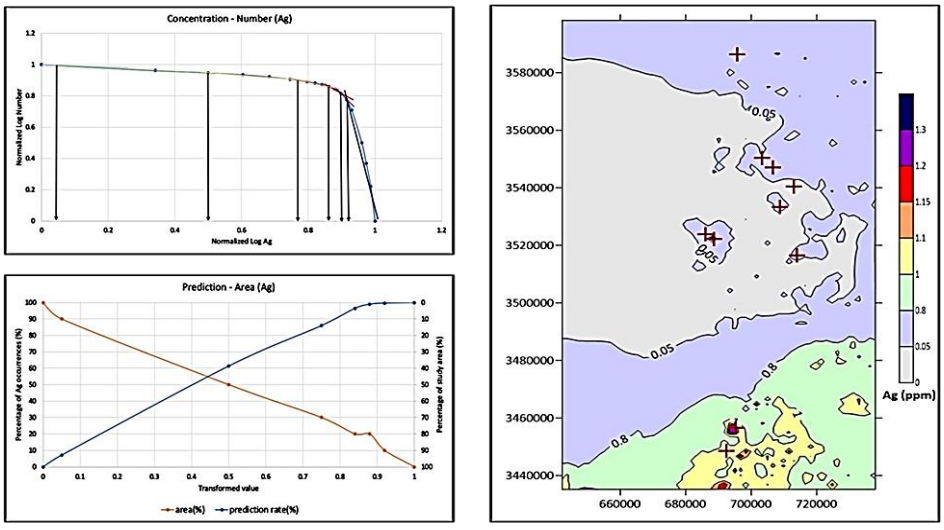

Figure 8. Silver geochemical distribution map, (a) full logarithmic graph of Concentration-Number fractal, (b) Prediction-Area diagram, and (c) fractal-based classification map. The extraction weight is equal to 0.20067.

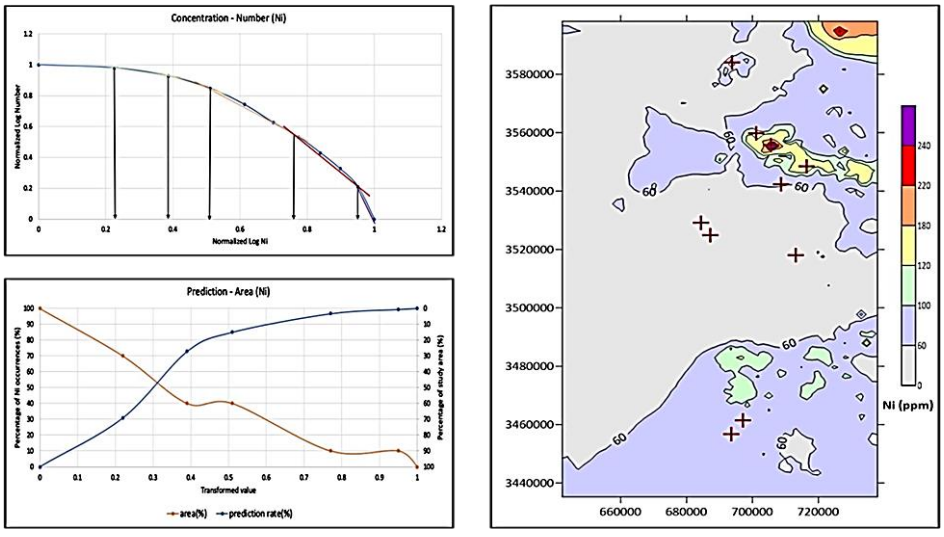

Figure 9. Nickel geochemical distribution map, (a) full logarithmic graph of Concentration-Number fractal, (b) Prediction-Area diagram, and (c) fractal-based classification map. The extraction weight is equal to 0.12014.

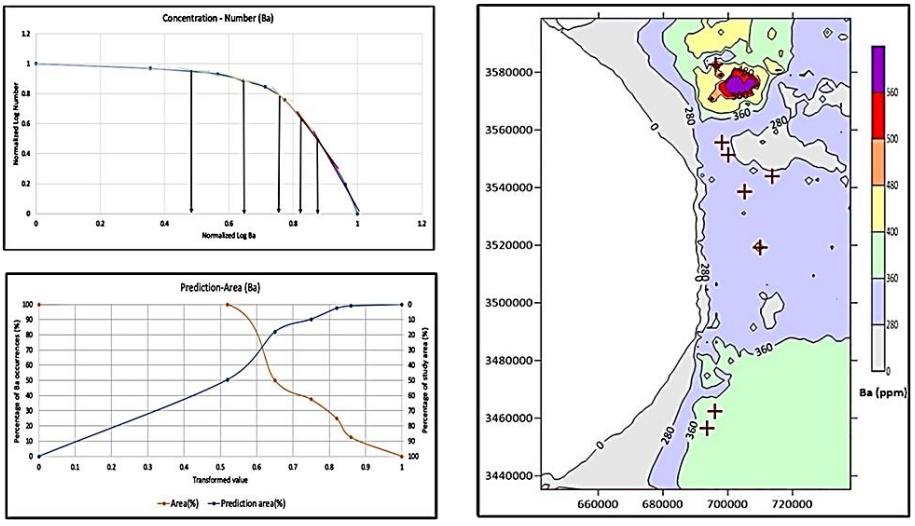

Figure 10. Barium geochemical distribution map, (a) full logarithmic graph of Concentration-Number fractal, (b) Prediction-Area diagram, and (c) fractal-based classification map. The extraction weight is equal to 0.94446.

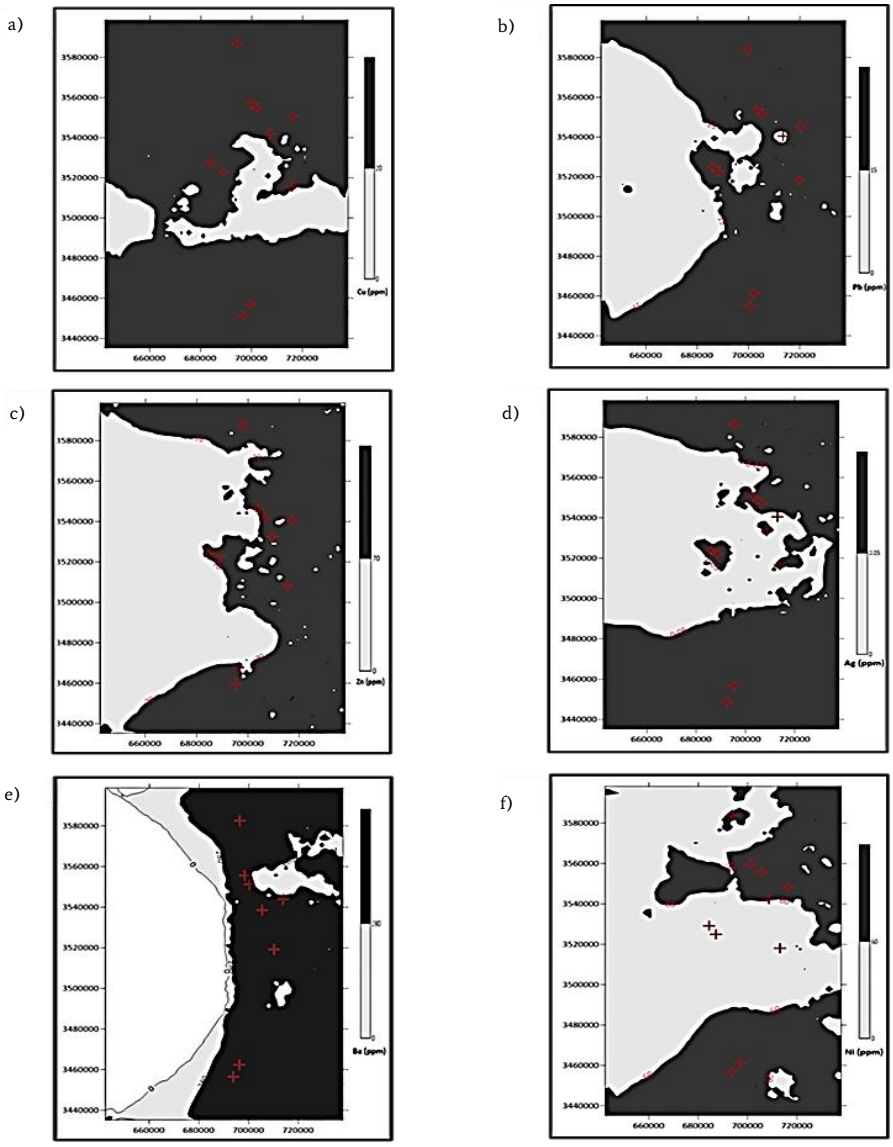

Figure 11. Geochemical distribution map of all elements in two classes, respectively for a) Copper, b) Lead, c) Zinc, d) Silver, e) Barium and f) Nickel.

prediction rate curve for the weight proof map classes and the percentage of occupied areas curve for the weight proof map classes. Usually, a fractal model is used to separate different populations/classes in a control/evidence map. In the P-A diagram of a given layer of an evidence map, if the intersection point shows a higher value on the left axis (i.e., higher prediction rate) compared to the P-A diagram of other control layers, it means that its layer has a lower value on the right axis (i.e., smaller occupied area). Since the sum of the mine deposit prediction rates and the area occupied at the intersection point is 100, if two curves intersect at a location above the P-A diagram of a control layer (relative to other evidence layers), it indicates a smaller area containing the number of mineral deposits, which means that there is a higher probability of mineral occurrence for this class in the evidence map [24].

The P-A diagram of the Cu variables, shown in Figure 5b, predicts 44% of the study area as the desired region and 56% of the known Cu events. The P-A diagram of the Pb element, shown in Figure6b, predicts 45% of the study area with an ore prediction rate of 55%. Figure 7b predicts 35% of the study area with a 65% ore prediction rate for the Zn element. In the case of the Ag element, 45% of the study area is predicted with a prediction rate of 55%, which for the Ni and Ba elements is 47% of the region with a prediction rate of 53% for nickel and 72% of the region with a prediction rate of 28%, for barium, respectively. The extracted parameters at the intersections of P-A components for geochemical evidence are given in Table 5.

In this study, the values in the evidence maps are converted using a logistic function to the range [0,1]. Then, the weight of individual evidence maps is determined using the P-A diagram by this data-driven method [24]. Based on the concentration-number fractal method, six geochemical maps of Cu, Pb, Zn, Ag, Ba, and Ni were prepared. The multi-class index overlay map of the copper through the integration of all the proven layers is shown in Figure 12c. The integrated map has three classes (Figure 12a), with the lowest class containing values 0-0.64 (light blue) and the highest class 0.92-1 (light green). Based on the intersection point in Figure 12b, the MPM output occupies 25% of the study area with an ore prediction rate of 75%. The weight of the composite evidence map is more than that of other geochemical layers (Table 5), showing its superiority over other evidence maps. The weights are calculated using the natural logarithm of the ore's forecast/prediction rate to the occupied area at the intersection. This means that the intersection point in the MPM P-A diagram has a higher value (75%> 72, 65, 56, 55, 55, and 53%) than other indicators.

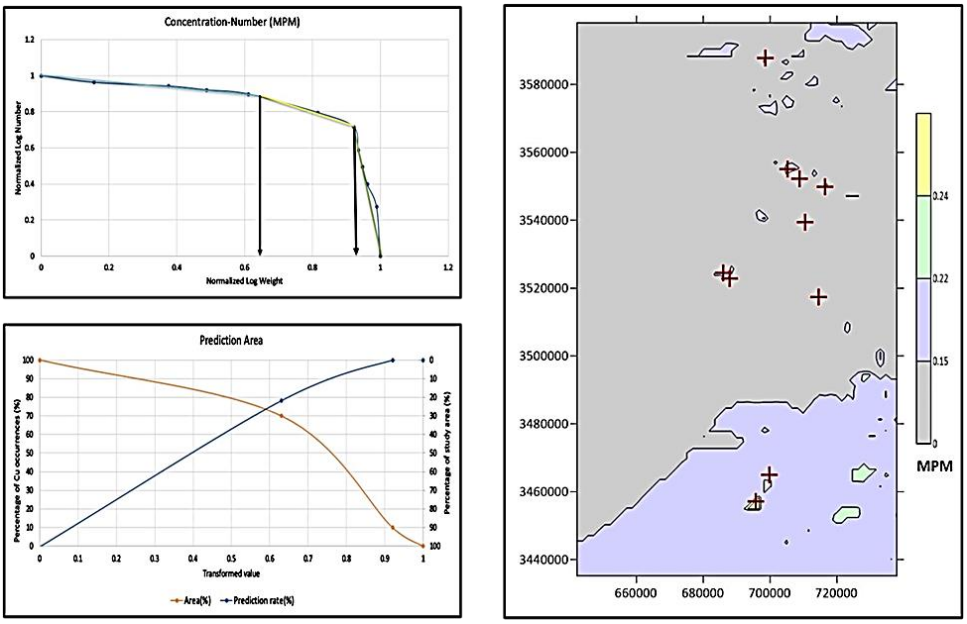

Figure 12. Copper geochemical potential map based on multi-class index overlay method, (a) full logarithmic fractal diagram of Concentration-Number, (b) Prediction-Area diagram, and (c) Fractal-based classification map. The extraction weight is equal to 1.09861.

Table 5. Parameters and weights derived from the Prediction-Area curve for Evidence layers.

Elements	Area	Prediction	Normalize	Log (A/P)	Weight
Cu	44	56	1.2728	0.10473	0.24116
Pb	45	55	1.2222	0.08715	0.20067
Zn	35	65	1.8571	0.26884	0.61904
Ag	45	55	1.2222	0.08715	0.20067
Ba	28	72	2.5714	0.41017	0.94446
Ni	47	53	1.1277	0.05218	0.12014
MPM	25	75	3.0000	0.47712	1.09861

4. Conclusion

In fractal models, highly enriched mineral areas have a strong and significant relationship with the desired areas in the synthesized evidence map. The main anomalous regions are Cu, Pb, Zn, Ag, Ba, and Ni in the southern, central, and southeastern parts of the region with minimal areas in the northern part. The geological map shows that the abnormal areas are mainly in the Middle to Upper Eocene rocks. The southern and southwestern regions, which show the most anomalies, are common in dacite, andesite, basaltic, and granodiorite rocks with diorite and monzonite. In the middle part of the study area, anomalies in basalt, andesite, and dacite rocks are observed, which are all related to the Eocene era. However, some signs of copper enrichment can be seen in the granites of this part. There are signs of copper enrichment in the northern part of the region. The type of host rocks, which are related to the Neogene and pyroclastic types, along with apatite and some rocks from the Lower Neogene era, has formed different types of reserves. The Correlation between rock types and elemental distribution by the C-N method shows that andesite, basalt, and dacite are related to copper anomalies in all parts of the study area.

According to the results of integrated evidence layers and maps, some areas can be introduced as new anomalies, especially in the southeastern part of the region, in the study area.

Another noticeable point is that a hybrid evidence map with a multi-class index overlay map can depict desirable areas with higher performance compared to any evidence. Therefore, this criterion can be placed in an exploratory database as a robust footprint in porphyry copper exploration. It needs to combine geological and geophysical criteria to reinforce the final synthesized evidence map with higher ore prediction rates and less occupied areas as the desirable regions.

Acknowledgment

The authors are grateful to the Geological Survey of Iran for data provision. Two anonymous reviewers are also appreciated for their constructive comments which helped the improvement of this work.

REFRENCES

[1] Lowell, J. D and Guilbert, J. M. (1970). Lateral and vertical alteration-mineralization zoning in porphyry ore deposits: Economic Geology, v. 65, p. 373-408.

[2] Harris J, Wilkinson L, Grunsky E, Heather K, Ayer J (1999). Techniques for analysis and visualization of lithogeochemical data with applications to the Swayze greenstone belt, Ontario, Journal of Geochemical Exploration 67:301-334.

[3] Cheng Q (1999). Spatial and scaling modelling for geochemical anomaly separation, Journal of Geochemical exploration 65:175-194.

[4] Cheng, Q., Agterberg, F. and Bonham-Carter, G., (1996) A spatial analysis method for geochemical anomaly separation. Journal of Geochemical exploration, 56: 183-195.

[5] Ghavami-Riabi, R., Seyedrahimi-Niaraq, M., Khalokakaie, R. and Hazareh, M., (2010) U-spatial statistic data modeled on a probability diagram for investigation of mineralization phases and exploration of shear zone gold deposits. Journal of Geochemical exploration, 104: 27-33.

[6] Darabi-Golestan, F., Ghavami-Riabi, R., Khalokakaie, R., Asadi-Haroni, H., Seyedrahimi-Niaraq, M., 2013, Interpretation of lithogeochemical and geophysical data to identify the buried mineralized area in Cu-Au porphyry of Dalli-Northern Hill. Arabian Journal of Geosciences, 6:4499-4509.

[7] Seyedrahimi-Niaraq, M., Hekmatnejad, A., (2020). The efficiency and accuracy of probability diagram, spatial statistic and fractal methods in the identification of shear zone gold mineralization: a case study of the Saqqez gold ore district, NW Iran. Acta Geochimica, https://doi.org/10.1007/s11631-020-00413-7.

[8] Qiuming C (2000). Multifractal theory and geochemical element distribution pattern, Earth Science-Journal of China University of Geosciences 25:311-318.

[9] Hawkes RAW, Webb HE (1979). Geochemistry in mineral exploration, 2nd edn. Academic Press, New York, 657 pp.

[10] Li, C.J., Ma, T.H., Shi, J.F., (2003). Application of a fractal method relating concentration and distances for separation of geochemical anomalies from background. J Geochem Explor 77: 167–175.

[11] Mandelbrot, B.B., (1983). The Fractal Geometry of Nature. WH Freeman, San Francisco, pp 1-468.

[12] Cheng, Q., Agterberg, F.P., Ballantyne, S.B., (1994). The separation of geochemical anomalies from background by fractal methods. J Geochem Explor 51: 109–130.

[13] Farhadi, S., Afzal, P., Boveiri Konari, M., Daneshvar Saein, L., Sadeghi, B., 2022. Combination of Machine Learning Algorithms with Concentration-Area Fractal Method for Soil Geochemical Anomaly Detection in Sediment-Hosted Irankuh Pb-Zn Deposit, Central Iran. Minerals 12 (6), 689.

[14] Koohzadi, F., Afzal, P., Jahani, D., Pourkermani, M., 2021. Geochemical exploration for Li in regional scale utilizing Staged Factor Analysis (SFA) and Spectrum-Area (S-A) fractal model in north central Iran. Iranian Journal of Earth Sciences 13, 299-307.

[15] Pourgholam, M.M., Afzal, P., Adib, A., Rahbar, K., Gholinejad, M., 2022. Delineation of Iron Alteration Zones using Spectrum-Area Fractal Model and TOPSIS Decision-Making Method in Tarom Metallogenic Zone, NW Iran. Journal of Mining and Environment (JME) 13, 2, 503-525.

[16] Shahbazi, S., Ghaderi, M., Afzal, P., 2021. Prognosis of gold mineralization phases by multifractal modeling in the Zehabad epithermal deposit, NW Iran. Iranian Journal of Earth Sciences 13, 31-40.

[17] Torshizian, H., Afzal, P., Rahbar, K., Yasrebi, A.B., Wetherelt, A., Fyzollahhi, N., 2021. Application of modified wavelet and fractal modeling for detection of geochemical anomaly. Geochemistry, 81(4), 125800.

[18] Nabilou, Afzal, P., M., Arian, M., Adib, A., Kheyrollahi, H., Foudazi M., Ansarirad, P., 2022. The relationship between Fe mineralization and the magnetic basement structures using multifractal modeling in the Esfordi and Behabad Areas (BMD), central Iran. Acta Geologica Sinica-English Edition. 96(2), 591–606.

[19] Mahdizadeh, M., Afzal, P., Eftekhari, M., Ahangari, K., 2022. Geomechanical zonation using multivariate fractal modeling in Chadormalu iron mine, Central Iran. Bulletin of Engineering Geology and the Environment 81 (1), 1-11.

[20] Afzal, P., Fadakar Alghalandis, Y., Khakzad, A., Moarefvand, P., Rashidnejad Omran, N., (2011). Delineation of mineralization zones in porphyry Cu deposits by fractal concentration–volume modeling. J Geochem Explor 108: 220–232.

[21] Afzal, P., Dadashzadeh Ahari, H., Rashidnejad Omran, N., Aliyari, F., (2013). Delineation of gold mineralized zones using concentration-volume fractal model in Qolqoleh gold deposit, NW Iran. Ore Geology Reviews 55: 125-133.

[22] Delavar, S.T., Afzal, P., Borg, G., Rasa, I., Lotfi, M., Rashidnejad Omran, N., (2012). Delineation of mineralization zones using concentration-volume fractal method in Pb-Zn carbonate hosted deposits. J. Geochem. Explor. 118, 98–110.

[23] Zuo, R., (2011). Decomposing of mixed pattern of arsenic using fractal model in Gangdese belt, Tibet, China. Appl. Geochem. 26, S271–S273.

[24] Zuo, R., Wang, J., (2016). Fractal/multifractal modeling of geochemical data: a review. J. Geochem. Explor. 164, 33–41.

[25] Panahi, A., Cheng, Q., & Bonham-Carter, G. F. (2004). Modelling lake sediment geochemical distribution using principal component, indicator kriging and multifractal power-spectrum analysis: a case study from Gowganda, Ontario. Geochemistry: Exploration, Environment, Analysis, 4(1), 59-70.

[26] Mirzaie, M., Afzal, P., Adib, A., Rahimi, E., & Mohammadi, G. (2020). Detection of zones based on ore and gangue using fractal and multivariate analysis in Chah Gaz iron ore deposit, Central Iran. Journal of Mining and Environment, 11(2), 453-466.

[27] Nyka¨nen, V., Lahti, I., Niiranen, T., & Korhonen, K. (2015). Receiver operating characteristics (ROC) as validation tool for prospectivity models—a magmatic Ni–Cu case study from the Central Lapland Greenstone Belt, Northern Finland. Ore Geology Reviews, 71, 853–860.

[28] Yousefi, M., & Carranza, E. J. M. (2015). Prediction–area (P–A) plot and C–A fractal analysis to classify and evaluate evidential maps for mineral prospectivity modeling. Computers & Geosciences, 79, 69-81.

[29] Carranza, E. J. M., & Laborte, A. G. (2016). Data-driven predictive modeling of mineral prospectivity using random forests: A case study in Catanduanes Island (Philippines). Natural Resources Research, 25, 35–50.

[30] Bonham-Carter, G. F., Agterberg, F. P., & Wright, D. F. (1989). Weights of evidence modelling: A new approach to mapping mineral potential. Statistical Applications in the Earth Sciences, 89, 171–183.nces, 85, 103-114.

[31] Yousefi, M., & Carranza, E. J. M. (2016). Data-driven index overlay and Boolean logic mineral prospectivity modeling in greenfields exploration. Natural Resources Research, 25, 3–18.

[32] Du, X., Zhou, K., Cui, Y., Wang, J., Zhang, N., & Sun, W. (2016). Application of fuzzy Analytical Hierarchy Process (AHP) and Prediction-Area (P-A) plot for mineral prospectivity mapping: A case study from the Dananhu metallogenic belt, Xinjiang, NW China. Arabian Journal of Geosciences, 9, 298.

[33] Gao, Y., Zhang, Z., Xiong, Y., & Zuo, R. (2016). Mapping mineral prospectivity for Cu polymetallic mineralization in southwest Fujian Province, China. Ore Geology Reviews, 75: 16–28.

[34] Nezhad, S. G., Mokhtari, A. R., & Rodsari, P. R. (2017). The true sample catchment basin approach in the analysis of stream sediment geochemical data. Ore Geology Reviews, 83, 127–134.

[35] Zhang, N., Zhou, K., & Du, X. (2017). Application of fuzzy logic and fuzzy AHP to mineral prospectivity mapping of porphyry and hydrothermal vein copper deposits in the Dananhu-Tousuquan island arc, Xinjiang, NW China. Journal of African Earth Sciences, 128, 84–96.

[36] Almasi, A., Yousefi, M., & Carranza, E. J. M. (2017). Prospectivityanalysis of orogenic gold deposits in Saqez-Sardasht Goldfield, Zagros Orogen, Iran. Ore Geology Reviews, 91,1066–1080.

[37] Roshanravan, B., Aghajani, H., Yousefi, M., & Kreuzer, O. (2019). An improved prediction-area plot for prospectivity analysis of mineral deposits. Natural Resources Research, 28(3), 1089-1105.

[38] Kreuzer, O. P., Yousefi, M., & Nykänen, V. (2020). Introduction to the special issue on spatial modelling and analysis of ore forming processes in mineral exploration targeting. Ore Geology Reviews 119, 103391

[39] Yousefi, M., Carranza, E. J. M., Kreuzer, O. P., Nykänen, V., Hronsky, J. M. A., & Mihalasky, J. M. A. (2021). Data analysis methods for prospectivity modelling as applied to mineral exploration targeting: State-of-the-Art and Outlook. Journal of Geochemical Exploration 229, 106839.

[40] Bishop, C. M. (2006). Pattern recognition and machine learning. springer.

[41] Aghanabati, A. (2005). Geology of Iran. Geological Survey of Iran, 586 p.

[42] Behrouzi A., Nazer N. Kh. (1992). Geological Map of Basiran, 1:100000. GSI, Tehran.

[43] Tahernejad, M. M., Khalo Kakaei, R., & Ataei, M. (2018). Analyzing the effect of ore grade uncertainty in open pit mine planning; A case study of Rezvan iron mine, Iran. International Journal of Mining and Geo-Engineering, 52(1), 53-60.

[44] Riemann, C., Filzmoser, P., & Garrett, R. G. (2002). Factor analysis applied to regional geochemical data: problems and possibilities. Applied geochemistry, 17(3), 185-206.

[45] Nazarpour, A., Omran, N. R., & Paydar, G. R. (2015). Application of multifractal models to identify geochemical anomalies in Zarshuran Au deposit, NW Iran. Arabian Journal of Geosciences, 8(2), 877-889.

[46] Berberian M., & King G. C. P. (1981). Towards the Paleogeography and tectonic evolution of Iran. Canadian Journal of Earth Sciences 18, 210-265.

[47] Khalifani, F., Bahroudi, A., Barak, S., & Abedi, M. (2019). An integrated Fuzzy AHP-VIKOR method for gold potential mapping in Saqez prospecting zone, Iran. Earth Observation and Geomatics Engineering, 3(1), 21-33.

[48] Grant, A. (1990). Multivariate statistical analyses of sediment geochemistry. Marine Pollution Bulletin, 21(6), 297-299.

[49] Zumlot, A. B. T. (2012). Multivariate statistical approach to geochemical methods in water quality factor identification; application to the shallow aquifer system of the Yarmouk Basin of north Jordan. Research Journal of Environmental and Earth Sciences, 4(7), 756-768.

[50] Ammar, F. H., Chkir, N., Zouari, K., Hamelin, B., Deschamps, P., & Aigoun, A. (2014). Hydro-geochemical processes in the Complexe Terminal aquifer of southern Tunisia: An integrated investigation based on geochemical and multivariate statistical methods. Journal of African Earth Sciences, 100, 81-95.

[51] Karar, K., Gupta, A. K., Kumar, A., & Biswas, A. K. (2006). Characterization and identification of the sources of chromium, zinc, lead, cadmium, nickel, manganese and iron in PM 10 particulates at the two sites of Kolkata, India. Environmental Monitoring and Assessment, 120(1-3), 347-360.

[52] Sprovieri, R., Thunell, R., & Howe, M. (2020). Paleontological and geochemical analysis of three laminated sedimentary units of late Pliocene-early Pleistocene age from the Monte San Nicola section in Sicily. Rivista Italiana di Paleontologia e Stratigrafia, 92(3).

[53] Nabatian, G., Rastad, E., Neubauer, F., Honarmand, M., & Ghaderi, M. (2015). Iron and Fe–Mn mineralisation in Iran: implications for Tethyan metallogeny. Australian Journal of Earth Sciences, 62(2), 211-241.

[54] Hirst, D. M. (1974). Geochemistry of Sediments from Eleven Black Sea Cores: Geochemistry.

[55] Malinowski, E. R., & Howery, D. G. (1980). Factor analysis in chemistry (p. 10). New York: Wiley.

[56] Wu, R., Chen, J., Zhao, J., Chen, J., & Chen, S. (2020). Identifying Geochemical Anomalies Associated with Gold Mineralization Using Factor Analysis and Spectrum–Area Multifractal Model in Laowan District, Qinling-Dabie Metallogenic Belt, Central China. Minerals, 10(3), 229.

[57] Richards, J., Wilkinson, D., & Ullrich, T. (2006). Geology of the Sari Gunay epithermal gold deposit, Northwest Iran. Econ. Geol. 101, 1455-1496.